https://doi.org/10.1007/s41230-025-4208-9

Optimizing mechanical performance and microstructural integrity in CaO-doped alumina ceramic cores by additive manufacturing

Zong-dong Hao[1, 2], Wei-zhe Tang[1, 2], *Rui Dou[1, 2], and **Li Wang[1, 2]

1. Jiangsu Key Laboratory of Advanced Food Manufacturing Equipment and Technology, School of Mechanical Engineering, Jiangnan University, Wuxi 214122, Jiangsu, China

2. Institute of Advanced Technology, Jiangnan University, Wuxi 214122, Jiangsu, China

Abstract: Alumina ceramics are crucial for high-performance applications, such as turbine blades, due to their excellent thermal stability and mechanical properties. However, existing fabrication methods often fail to balance strength, porosity, and dimensional precision. This study partially fills this research gap through a systematic investigation of calcium oxide (CaO) doping effects on alumina ceramic cores fabricated via ceramic stereolithography, with controlled doping ratios and sintering parameters. A ceramic paste was prepared using coarse and fine Al_2O_3 particles mixed with CaO as a sintering aid, followed by debinding and sintering to achieve optimal mechanical properties. The results show that CaO doping significantly enhances the flexural strength of alumina cores while maintaining porosity levels between 20% and 30% and controlling the sintering shrinkage rate to about 5%. Additionally, CaO doping alters the microstructure by inhibiting the transformation of spherical fine particles into flaky grains, improving sintering activity. However, as the CaO doping content increases, the bending strength increases, while the shrinkage rate of the material also tends to increase, resulting in a reduction in the overall porosity. This has a negative impact on the control of the manufacturing precision of turbine blades. Thus, although CaO doping improves strength and microstructure, achieving necessary dimensional control requires further optimization of doping content and sintering conditions.

Keywords: vat photopolymerization; alumina ceramic cores; CaO doping; mechanical properties; sintering shrinkage

CLC numbers: TG221 **Document code:** A **Article ID:** 1672-6421(2025)05-583-09

1 Introduction

Jet-engine turbine blades typically possess intricate cooling channels that are formed by ceramic cores during the casting process [1]. Ceramic cores for blade casting mainly devided into two types based on materials: silica-based cores and alumina-based cores. However, the thermal stability of silica cores is relatively low, and it easily reacts with the alloying elements (Al, Hf, C) at high temperatures [2]. Hence, silica cores are not appropriate for the high casting temperature of new-generation superalloys for high-performance hollow blades [3]. In contrast, alumina cores are more suitable for the high temperature (>1,550 °C) casting process of single crystal nickel-based superalloy hollow turbine blades due to their stable overall properties and excellent chemical stability [4, 5, 41].

However, the fabrication of ceramic cores is difficult due to the strict requirements for single-crystal nickel-based superalloy turbine blade castings. For instance, the shrinkage rate of ceramic cores must be low, so as to increase dimensional precision and avoid possible cracks due to large deformations. Besides, the different thermal expansion coefficients of alumina and metal can lead to thermal tearing, hence

***Rui Dou**

Male, Ph. D., Professor. His research interests primarily focus on frontier new materials and processes for ceramic stereolithography (SLA) additive manufacturing technology.

E-mail: ruidou@jiangnan.edu.cn

****Li Wang**

Male, Ph. D., Professor. His research interests primarily focus on frontier new materials and processes.

E-mail: liwang@jiangnan.edu.cn

Received: 2024-10-17; Revised: 2024-11-16; Accepted: 2024-11-29

proper porous structure of the alumina core is desired [6, 42]. Moreover, to resist mechanical and thermal impact during high temperature alloy casting and solidification processes, the ceramic core should have a moderate strength [4, 7, 8]. Finally, the sintering temperature of ceramic cores must be higher than the working temperature; besides, the core will continue to sinter during the blade casting process [4, 8, 43]. Consequently, the key characteristics of ceramic cores can be summarized as: a shrinkage of less than 5%; a proper porosity (>20%); a moderate strength (20 MPa–30 MPa); and a sintering temperature of higher than 1,550 °C [44].

The complexity of cooling channels, which directly affects the design of ceramic cores, is highly sought after in the development of more fuel-efficient engines [9, 10]. However, the conventional methods of alumina core manufacturing, namely hot injection molding and gel casting, not only require a long lead-time and expensive cost of tool manufacturing, but also the fabrication of molds is limited in geometric complexity [11, 12]. In contrast, additive manufacturing technology can fabricate ceramic cores without molds, which reduces expenses, shortens the leading time of design and manufacture, and shows great potential in fabricating intricate structures [13-15]. Compared to other additive manufacturing methods, vat photopolymerization (VPP) technology shows more advantages in the fabrication of ceramic cores with fine structures due to its higher dimensional precision [14, 16]. Tang et al. [17] discovered that the VPP technology was appropriate for the preparation of ceramic cores with low shrinkage and complicated structure, demonstrating the feasibility of VPP technology for the fabrication of ceramic cores. However, the flexural strength of low-shrinkage alumina cores can not meet the requirement of high-temperature casting of single-crystal blades. Hence, it is necessary to further improve the strength of alumina cores fabricated by VPP technology and maintain a low shrinkage and a proper porosity.

Recent studies suggest that sintering aids can be added into alumina cores to improve mechanical properties [18-20]. Considering that the sintering aids can influence the shrinkage of alumina cores, the objective of this work is to investigate the applicability of sintering aids doping for the additive manufactured alumina cores with a low shrinkage and a moderate strength. Several sintering aids elements are known in the literature, such as MgO, CaO, SiO_2, etc [21]. It was reported that the addition of sintering aids exhibited a series of excellent properties of alumina cores such as high strength, good high-temperature resistance [22, 23]. Although SiO_2 and MgO are commonly used for the sintering aids of alumina, these dopants have a few drawbacks. For instance, Liu et al. [24] improved the strength of alumina cores by doping with SiO_2, but the shrinkage in the *z*-direction reached 7% after sintering at 1,500 °C for 3 h. Additionally, SiO_2 and MgO can react with the key elements in advanced superalloys, which can impair thermal stability [25]. CaO is commonly added to alumina to improve sintering process. Several reasonable mechanistic explanations for the beneficial effect of CaO include solute-drag, particle-pinning, modification of defect chemistry, increase of surface diffusivity, modification of viscosity, surface tension and wettability of liquid phase, and modification of interfacial properties [26]. Johnson et al. [27, 28] proposed that CaO-doped alumina eliminated the migration of pores from grain boundaries after sintering, thus inhibiting grain growth, which resulted in improved mechanical properties of the sintered alumina. Moreover, Bateman et al. [29] concluded that the presence of liquid phase after sintering of CaO-doped alumina promoted mass transfer and thus promoted sintering densification. It is also revealed that CaO doping can cause the calcium ions to segregate at grain boundaries, thus strengthening grain boundaries and improving the mechanical properties of alumina [30, 31]. All these theories conclude that there is no doubt about the enhancement of CaO for alumina. Although some studies have demonstrated that CaO doping can enhance the strength of alumina cores, the excessive shrinkage observed in these strengthened cores fails to meet the requirements for blade casting applications [19, 32]. Consequently, the applicability of CaO dopant in the fabrication of porous and low-shrinkage alumina cores was evaluated in this study.

For this purpose, alumina cores were successfully manufactured by reinforcing CaO-doped alumina using the VPP technology. The microstructure, elemental distribution, phase composition, and properties of alumina cores with different CaO contents have been systematically investigated. Microstructural analyses and flexural strength tests were performed to investigate the effect of CaO on the mechanical performance and the strengthening mechanism of the alumina cores.

2 Experiment

2.1 Fabrication of green samples

Coarse Al_2O_3 particles (3.96 g·cm^{-3}, D_{50}=5 μm, Aladdin, China) and fine Al_2O_3 particles (3.96 g·cm^{-3}, D_{50}=500 nm, Aladdin, China) were used as the raw material to prepare the Al_2O_3 ceramic paste. CaO (3.32 g·cm^{-3}, 500 nm, Aladdin, China) was employed as sintering aid. The samples were prepared by mixing the particles in specific ratios, as shown in Table 1.

The vat photopolymerization pastes consisted of coarse and fine alumina powders in a 2:1 weight ratio, with HDDA (1.01 g·cm^{-3}, Aladdin, China) as the photosensitive resin, Carbomer 940 (Aladdin, China) as the thickening agent, and TPO (1.17 g·cm^{-3}, Guangzhou Lihou Trading Co., Ltd., China) and KOS110 (Guangzhou Kangoushuang Trade Co., Ltd., China) as the photoinitiator and dispersant. The mixture was then ball-milled for 12 h at 300 rpm. The final formulation resulted in a paste with a solid content of 65%. Finally, alumina green bodies were fabricated from the pastes using a commercial ceramic 3D printer (3D Ceram C900, France). To ensure manufacturing quality and efficiency, the printing thickness per layer was set at 50 μm.

Table 1: Formula of ceramic samples with different CaO contents

Sample number	Sintering aids CaO (wt.%)
C-1	1
C-2	2
C-3	3

2.2 Debinding and sintering process

Debinding and sintering are crucial steps in ceramic core preparation, with the sintering process determining the final product quality. Firstly, the cleaned alumina green bodies were dried either on the surface or entirely to remove moisture, followed by debinding to eliminate organic materials. This step was performed in air at a heating rate of 1 °C·min^{-1}. To prevent cracking from an excessive heating rate, the temperature was maintained at 160 °C, 200 °C, 300 °C, 400 °C, and 450 °C for 1 h each, followed by at 800 °C kept for 1 h before cooling to room temperature at 5 °C·min^{-1}. The debinded samples were sintered in air using a muffle furnace at 1,550 °C, 1,600 °C, and 1,650 °C, with a 4 h holding time at each temperature. The heating rate was set to 5 °C·min^{-1}, and the samples were cooled to room temperature in the furnace after sintering.

2.3 Characterization

The dimensions of the ceramic samples: length (X direction), width (Y direction), and height (Z direction), were measured before and after sintering using a digital caliper. Ten samples were taken from each group, and the average value was calculated. The linear shrinkage rate (Δl) was calculated using Eq. (1):

$$\Delta l = \frac{l_1 - l_2}{l_1} \times 100\% \quad (1)$$

where l_1 is the measured dimension of the sample before sintering, and l_2 is the measured dimension of the sample after sintering.

In this experiment, the density and porosity of sintered Al_2O_3 ceramic samples were determined using the Archimedes displacement method. An analytical balance (ME 104/02, 0.0001 g, Mettler-Toledo Instruments, Shanghai) with an accuracy of 0.0001 g was used to measure the mass of the sintered samples.

Rotational rheology experiment was performed using a rotational rheometer equipped with parallel plate fixtures (25 mm in diameter) and a fixture gap set to 0.1 mm. The test temperature was set to 25 °C and maintained by the built-in control system to ensure stability. To ensure uniform temperature distribution, the paste was kept in the lab environment for at least 1 h before testing to reach thermal equilibrium.

The microstructure of the alumina ceramic samples was observed using scanning electron microscopy (Evo18, Carl Zeiss, Germany). Morphological changes in alumina and calcium oxide particles, along with fracture characteristics and porosity distribution, were analyzed.

3 Results and discussion

3.1 Rheological properties

In previous work [17], the formulation of graded alumina materials was investigated, converting the slurry into a ceramic paste exhibiting Bingham pseudoplastic behavior. The paste, with a solid content of 65%, demonstrated shear thinning properties and yield stress. As the CaO doping content increases, the actual solid content of the alumina paste also rises. As shown in Fig. 1(a), the apparent viscosity increases with the rise in CaO doping content. The paste's viscosity is influenced by the solid content, described by the Krieger-Dougherty model:

$$\mu = \mu_0 \left(1 - \frac{\beta\mu}{\varphi_m}\right)^{-[\mu]\varphi_m} \quad (2)$$

where, μ represents the viscosity of the ceramic paste (Pa·s), while μ_0 denotes the resin viscosity (Pa·s). β is the effective packing factor, indicating how the thickness of the dispersant adsorption layer influences viscosity. The intrinsic viscosity $[\mu]$ depends on the particle geometry, with a value of 2.5 for spherical particles. φ is the actual solid content of the paste, and φ_m represents the maximum solid content, which is determined by the particle size distribution of the ceramic particles. After doping with CaO, similar to the effect of fine particle doping, the fine particles fill the gaps between coarse particles, increasing the solid content and modifying the gradation ratio. Consequently, as the amount of CaO increases, the apparent viscosity of the alumina paste rises. As shown in Fig. 1(b), when varying amounts of CaO are added to the alumina paste, the relationship between shear stress and shear rate exhibits a curved trend, rather than a linear trend. This indicates that the doped alumina paste behaves as a non-Newtonian fluid. Additionally, Fig. 1(b) demonstrates that, regardless of CaO content, the shear stress of the alumina slurry does not reach zero, indicating a degree of shape retention, characteristic of a Bingham fluid. Furthermore, the non-linear relationship between shear stress and shear rate indicates that the alumina paste exhibits shear thinning behavior, confirming its characteristics as a Bingham pseudoplastic fluid.

$$\tau = \tau_0 + K\left(\frac{\partial u}{\partial y}\right)^n \quad (3)$$

In Eq. (3), τ represents shear stress [as shown in the Fig. 1(a)] in Pa, and $(\partial u/\partial y)$ denotes the shear rate in s^{-1}. τ_0 is the yield stress of the paste (obtained by fitting) in Pa. K is the consistency index (also obtained by fitting), measured in (Pa·s)^n. When K equals 0, it represents an ideal fluid. K<1 indicates a low-viscosity fluid, such as water, while K>1 means viscosity increases with K. The flow behavior index n (obtained by fitting) signifies shear thickening when n>1 and shear thinning when n<1. Equation (3) was used to analyze and fit the shear stress data of alumina pastes with varying levels of CaO doping (fitting R^2= 0.95). The fitted K values are 42.31, 45.65,

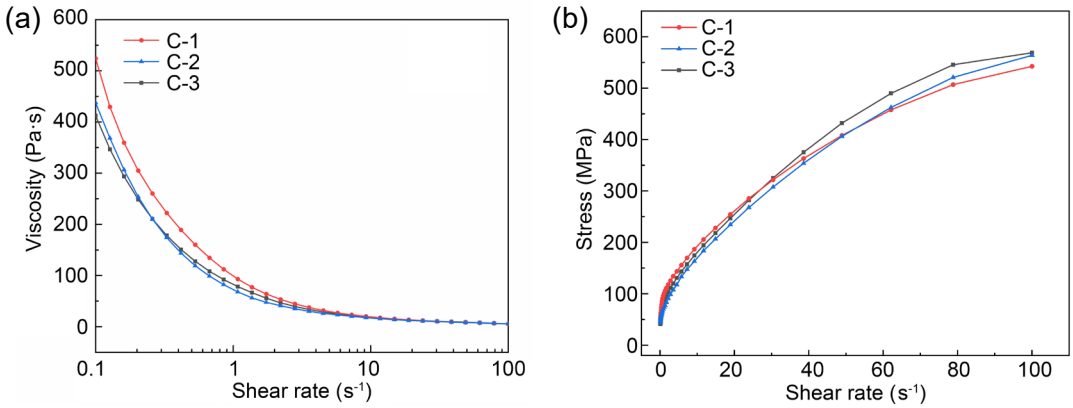

Fig. 1: Effect of shear rate on viscosity (a) and shear stress (b) of alumina paste doped with CaO

and 57.79, all exceeding 1, showing that viscosity increases with higher CaO doping. Additionally, the fitted n values are 0.563, 0.594, and 0.599, all below 1, confirming the shear thinning behavior of the alumina paste.

When the applied stress is below τ_0, the paste behaves like a solid, undergoing elastic deformation without flowing. In contrast, when the applied stress exceeds τ_0, the paste begins to flow viscously. Using Eq. (3) for fitting, the yield stresses of the three CaO-doped pastes are 36.49 Pa, 40.79 Pa, and 46.06 Pa, demonstrating that yield stress increases with an increase in CaO doping amount.

3.2 Effect of CaO on microstructure of alumina

At a sintering temperature of 1,550 °C, the morphology of some fine Al_2O_3 particles begins to change, as shown in Fig. 2(a), with spherical alumina particles transforming into flaky particles. These flaky particles feature flat top and bottom surfaces, along with curved side surfaces. Sintering reactions occur where the curved side surfaces make contact or where they meet the flat surfaces. In contrast, it is challenging for the flat surfaces to sinter together due to a weaker driving force and a larger atomic diffusion range, leading to a slower sintering rate. As a result, during the sintering process, these regions connect to form an integrated structure with a central cavity, as shown in Fig. 2(b). Pores remain within the internal spaces formed by the flaky grains, and this hollow structure preserves the high porosity of the alumina core after high-temperature sintering. In contrast, coarse particles are less likely to fully sinter due to their larger radius of curvature and lower specific surface area, which decrease the sintering driving force [33]. Therefore, the particle size of alumina ceramic powder is a key factor affecting the sintering process.

When the sintering reaction of alumina ceramic particles is fully initiated, grain boundaries form, resulting a reduction in the pores between particles and promoting ceramic densification. During this process, the grain size increases, accompanied by the migration of pores and grain boundaries, grain neck growth, and ceramic shrinkage, as shown in Fig. 2(c). Coarse particles are difficult to sinter, and therefore, they typically do not participate in the sintering reaction or form grain boundaries and grain necks, which hinders the densification process. Thus, alumina ceramics produced via the gradation method primarily depend on the sintering activity of fine particles and the influence of coarse particles on densification. However, coarse particles can inhibit sintering progression, delaying densification, preserving the pore structure, and controlling the post-sintering shrinkage rate.

SEM microstructures of alumina samples with varying CaO doping contents (0wt.%, 1wt.%, 2wt.%, and 3wt.%), sintered at 1,550 °C, are shown in Figs. 3(a–d). As the CaO content increases, the transformation of fine alumina particles into flake-like particles gradually decreases. In Fig. 3(d), almost no flake-like grains are observed, with the fine alumina particles remaining spherical. These results indicate that CaO doping inhibits the transformation of fine alumina particles into flake-like structures, reducing the formation of hollow structures and lowering porosity.

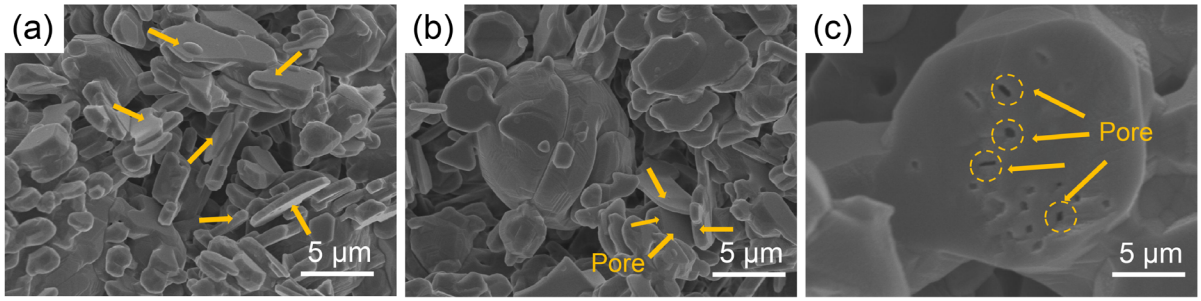

Fig. 2: Morphology of fine particles of alumina sintered at 1,550 °C: (a) morphology of fine particles; (b) pores between flake crystals; (c) morphology of coarse particles

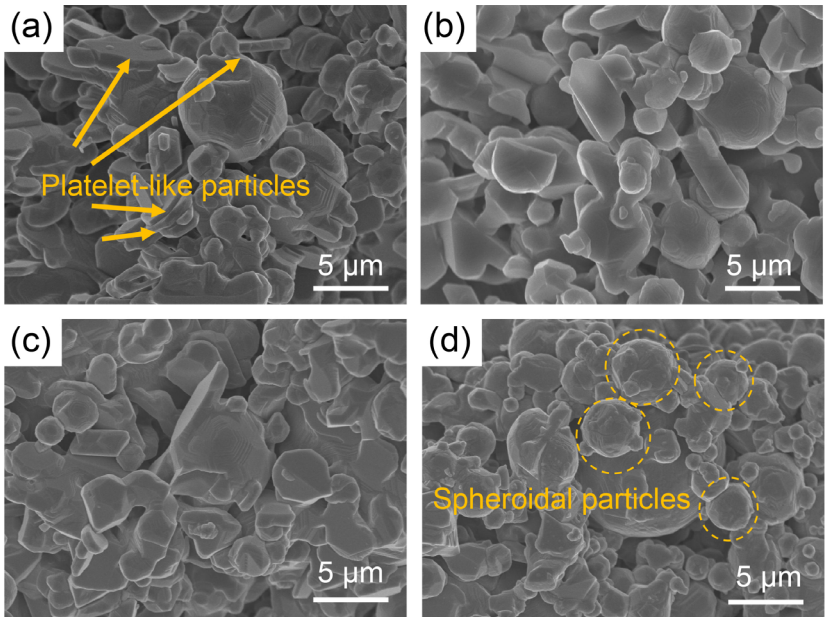

Fig. 3: Morphology of alumina grains with different doping levels at 1,550 °C: (a) 0wt.%; (b) 1wt.%; (c) 2wt.%; (d) 3wt.%

In general, doping CaO into alumina undergoes a sintering reaction through solid-phase sintering. During solid-phase sintering process, there are mainly two exchange mechanisms between Ca^{2+} and Al^{3+}. One mechanism is that two Ca^{2+} ions replace two Al^{3+} ions, creating an oxygen vacancy [45,46]. The resulting oxygen vacancies introduce lattice defects, affecting crystal stability, while the additional ions influence crystal growth and arrangement. These two factors ultimately influence the sintering behavior. Additionally, two ions exchange mechanisms increase the oxygen diffusion coefficient while reduce the Al^{3+} diffusion coefficient. The Al^{3+} diffusion coefficient describes the movement rate of Al^{3+} within the alumina crystal, significantly impacting the sintering process. As the CaO doping content increases, the Al^{3+} diffusion coefficient decreases, slowing the outward diffusion of Al^{3+} from the particle surface or interior, thereby inhibiting the bonding between crystal particles.

As shown in Fig. 4, smaller fine particles are closely attached to the surfaces of larger coarse particles, resulting in grain growth and changes in particle morphology. The labels in Fig. 4 indicate that the fine particles are randomly distributed on the surfaces of the coarse particles, forming protruding structures. As shown in Fig. 4(c), this structure prevents direct contact between particles, maintaining a gap between them and creating a unique porous structure on the particle surface. Based on the sintering morphology described above, this porous structure formed by the protrusions preserves the porosity of the ceramic cores even after high-temperature sintering. Furthermore, as the CaO content increases, the number of fine particles attached to the coarse particles also increases. This may be due to the increase in CaO altering the sintering behavior of fine alumina particles, inhibiting their transformation into flake-like structures. This reduction in planar structures increases the likelihood of contact between spherical fine alumina particles and coarse particles, resulting in more protrusions on the coarse particle surfaces.

At 1,550 °C, 1,600 °C, and 1,650 °C, both CaO (melting point: 2,572 °C) and Al_2O_3 (melting point: 2,072 °C) remain in the solid state, as their melting points are significantly higher than these reaction temperatures. CaO gradually diffuses to the surface of alumina particles through solid-state diffusion, facilitating the reaction at the interface. The formation of $CaO{\cdot}6Al_2O_3$ results in a solid layer of reaction products at the interface, strengthening the bond at the interface with alumina particles, increasing interface densification and improving interfacial strength, thereby enhancing the material's overall microstructure [34]. Hence, the strong ionic or covalent bonds at the $CaO{\cdot}6Al_2O_3$ and alumina interface reduce grain boundary

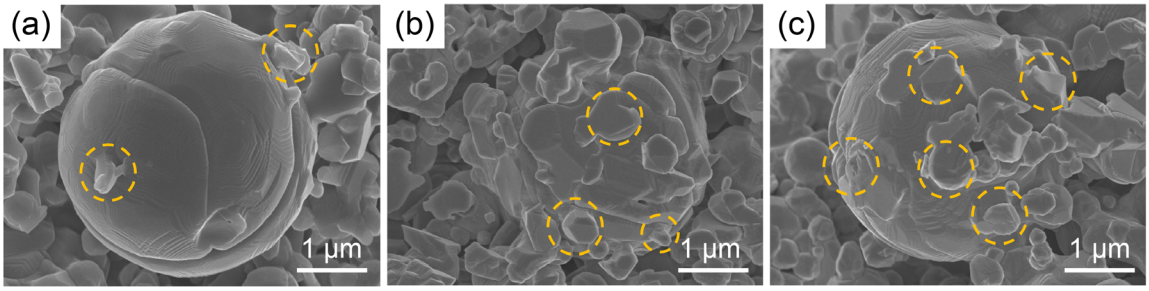

Fig. 4: Morphology of coarse alumina particles with different CaO doping levels after sintering at 1,550 °C: (a) 1wt.%; (b) 2wt.%; (c) 3wt.%

sliding, inhibiting crack propagation. Additionally, the thermal expansion coefficient of $CaO·6Al_2O_3$ is similar to that of Al_2O_3, minimizing stress concentration at the interface under high-temperature conditions, improving thermal stability, and reducing the risk of stress-induced cracking [35]. The intercrystalline $CaO·6Al_2O_3$ film, which inhibits the abnormal growth of alumina grains and prevents large alumina particles from transforming into plate-like crystals, helps maintain a more intact sphericity and plays a role in grain refinement. However, the formation of $CaO·6Al_2O_3$ creates a new phase interface between CaO and Al_2O_3, partially hindering further diffusion of Ca^{2+} and O^{2-}, thus slowing the subsequent reaction rate. As the reaction progresses, the $CaO·6Al_2O_3$ layer thickens, further limiting the diffusion path of the reactants. Due to the formation of a denser $CaO·6Al_2O_3$ layer at the grain boundaries between CaO and Al_2O_3, the overall porosity of the material is reduced to a certain extent.

In addition to the effect of CaO doping on ceramic properties, sintering temperature is a key factor, as it influences the diffusion behavior of Al^{3+} in Al_2O_3. Typically, increasing the sintering temperature accelerates Al^{3+} diffusion, enhances particle bonding, and thus increases the sintering rate. Conversely, lowering the sintering temperature slows the sintering rate. Thus, increasing the temperature promotes the densification process, reducing the porosity of alumina ceramic cores. As shown in Fig. 5, higher sintering temperatures reduce the transformation of fine alumina particles into flake-like structures and facilitate grain growth. For instance, alumina sintered at 1,650 °C has larger grains compared to alumina sintered at 1,550 °C. Grain growth occurs as alumina particles with larger curvature radii absorb smaller particles, causing grain boundaries to vanish and forming larger grains [36].

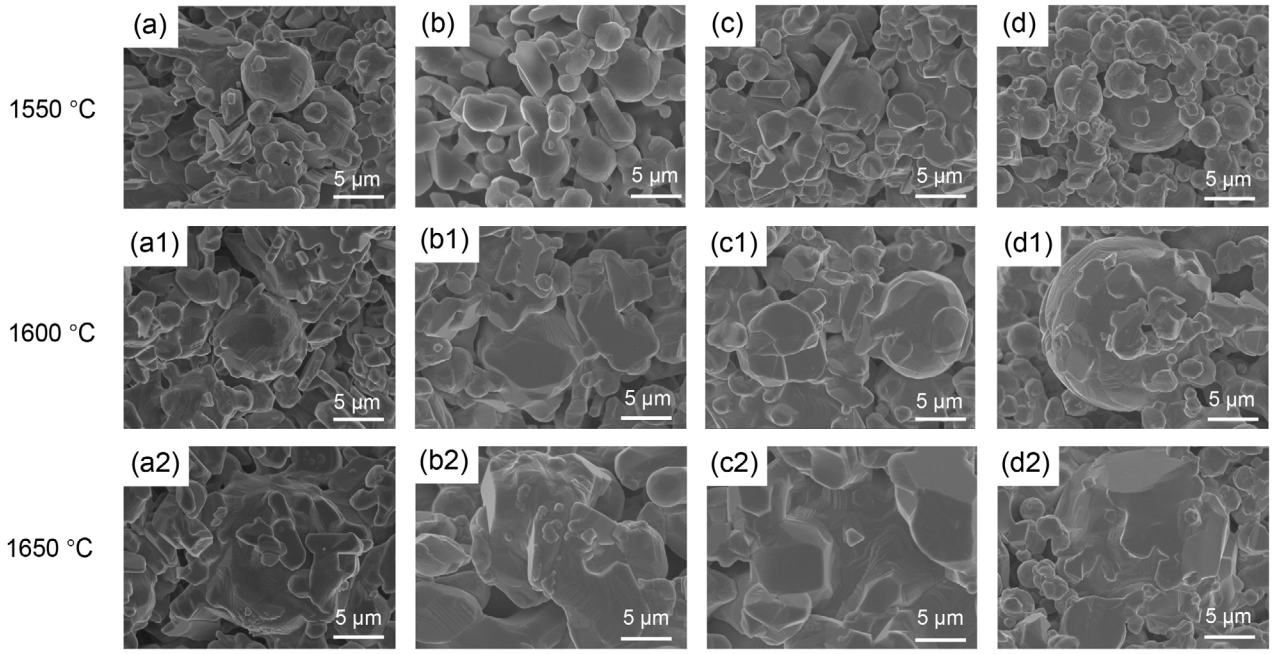

Fig. 5: Morphology of alumina ceramics with different sintering temperatures and CaO doping levels: (a)–(d) morphology of alumina with CaO doping levels of 0wt.%–3wt.% at 1,550 °C; (a1)–(d1) morphology of alumina with CaO doping levels of 0wt.%–3wt.% at 1,600 °C; (a2)–(d2) morphology of alumina with CaO doping levels of 0wt.%–3wt.% at 1,650 °C

At elevated temperatures, $CaO·6Al_2O_3$ becomes the dominant product of the reaction between CaO and alumina (Al_2O_3). Due to the low volume fraction of CaO, the reaction predominantly takes place at the interface between dispersed CaO particles and the alumina matrix, as shown in the red dotted circle in Fig. 6.

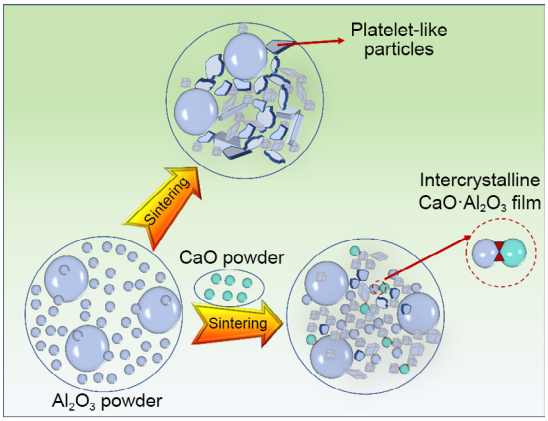

Fig. 6: Schematic representation of morphological evolution of Al_2O_3 particles

3.3 Mechanical properties of CaO-doped alumina

Figures 7(a, b, and c) illustrate the variation in shrinkage rate with CaO doping after sintering alumina samples at 1,550 °C, 1,600 °C, and 1,650 °C, respectively. As CaO doping increases and sintering temperature rises, the shrinkage rate in the *X, Y,* and *Z* directions gradually increases. Additionally, Fig. 8(a) summarizes the changes in flexural strength with CaO doping after sintering at the same temperatures. Higher CaO content

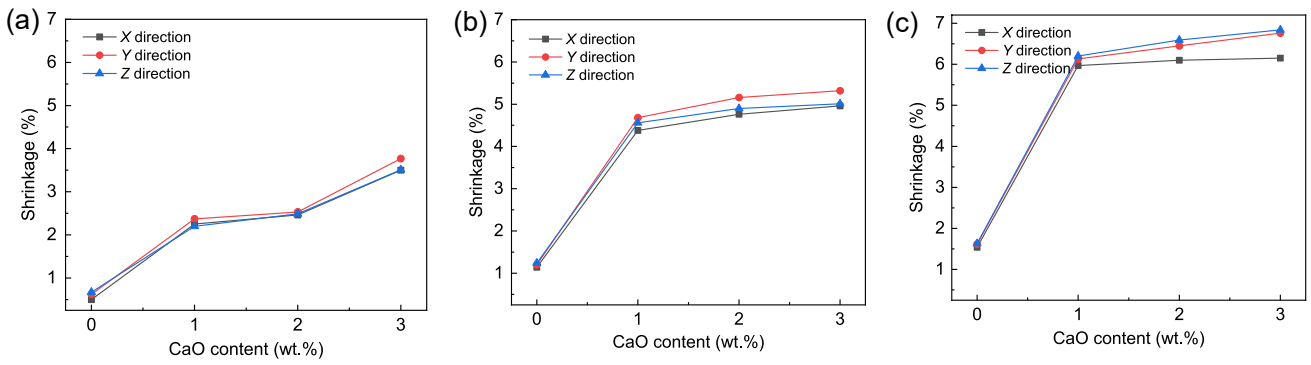

Fig. 7: Linear shrinkage rates of alumina ceramics with different CaO contents sintered at 1,550 °C (a); 1,600 °C (b); 1,650 °C (c)

and sintering temperature improve the mechanical properties of the ceramics. For instance, at a sintering temperature of 1,550 °C, the flexural strength of pure alumina (A-1) is 6.06 MPa. With increasing CaO doping, the flexural strength of C-1, C-2, and C-3 samples rises to 54.29 MPa, 58.94 MPa, and 69.15 MPa, respectively. Additionally, higher sintering temperatures improve flexural strength. When the temperature increases from 1,550 °C to 1,650 °C, the flexural strength of pure alumina, A-1, C-1, C-2, and C-3 increases from 6.06 MPa, 54.29 MPa, 58.94 MPa, and 69.15 MPa to 25.33 MPa, 134.89 MPa, 146.13 MPa, and 153.84 MPa, respectively. According to the sintering diffusion coefficient (D) equation, as shown in Eq. (4), the diffusion coefficient can be expressed as a function of temperature and material properties:

$$D = \frac{v\lambda^2}{6}\exp\left(\frac{-q}{kT}\right) \tag{4}$$

where, q represents the atomic diffusion activation energy, v is the atomic jump frequency, and λ denotes the atomic jump distance. Increasing the sintering temperature accelerates the atomic diffusion rate, enhances the densification process, and ultimately improves the flexural strength of materials.

In Fig. 8(a), it is evident that with CaO doping increases from 1wt.% to 2wt.% and 3wt.%, there is a clear improvement in the flexural strength of alumina samples. As the sintering temperature rises, the flexural strength of the C-1, C-2, and C-3 samples increases significantly. This suggests that at lower sintering temperatures, the sintering reaction between CaO and Al_2O_3 remains incomplete.

Increasing the sintering temperature accelerates atomic diffusion, enhancing the diffusion rates of Ca^{2+} and Al^{3+}, increasing the sintering rate, and promoting the reaction between CaO and pure alumina. Additionally, after raising the sintering temperature, the shrinkage rate of doped samples increases sharply, aligning with the changes in flexural strength [37, 38].

Based on the mechanical performance tests of sintered alumina samples with varying doping levels, as shown in Fig. 8(a), it is clear that CaO doping enhances the mechanical properties of alumina cores. However, the improvement in mechanical properties caused by CaO doping is excessively high. For example, at a sintering temperature of 1,550 °C, the flexural strength of C-1, C-2, and C-3 samples ranges from 54.29 MPa to 69.15 MPa, exceeding the required mechanical properties for casting cores. Furthermore, Fig. 8(b) shows the variation in porosity with CaO doping in alumina samples sintered at 1,550 °C, 1,600 °C, and 1,650 °C, which demonstrates an inverse trend compared to mechanical properties. The porosity of C-1, C-2, and C-3 samples ranges from 15.61% to 26.9%, failing to meet casting requirements for cores. These experimental results suggest that although CaO doping significantly enhances core performance, it adversely affects shrinkage rate and porosity, making it unsuitable for producing high-precision, shape-controlled cores.

As shown in Fig. 8, the results for flexural strength and porosity in CaO-doped alumina samples are presented. The sintering activity of fine particles, along with the enhanced sintering reaction between fine and coarse particles after CaO doping, leads to a denser system, thereby improving the flexural strength of alumina ceramic cores in an air atmosphere. Considering the shrinkage rate, porosity, and mechanical properties of alumina ceramic cores, it is evident that CaO doping alone cannot fully meet the high-precision requirements for shape and dimensional control. However, based on the observed trends, CaO doping leads to a steep increase in both flexural strength and shrinkage rate of alumina ceramics. Thus, although CaO doping significantly enhances the performance of alumina, it is unfavorable for controlling the shrinkage rate in alumina cores [39].

The research results show that the performance of graded VPP-alumina ceramic cores is influenced by CaO doping, and adjusting the doping levels significantly improves the overall performance of the cores. Previous studies indicate that particle size grading can effectively limit the shrinkage rate of alumina cores while maintaining high porosity [39, 40]. However, this approach remains limited by low flexural strength, which does not meet the casting requirement for single-crystal turbine blades. The main issue is attributed to the low sintering driving force of coarse particles in the grading system, which inhibits sintering activity and reduces the sintering rate. Consequently, higher sintering temperatures and longer holding times are necessary for greater densification. Doping with CaO as a sintering aid alters the exchange between Ca^{2+} and Al^{3+}, modifying the sintering behavior of fine alumina particles and inhibiting the transformation of spherical fine particles into flaky grains. The retained spherical fine particles enhance sintering activity, thereby improving flexural

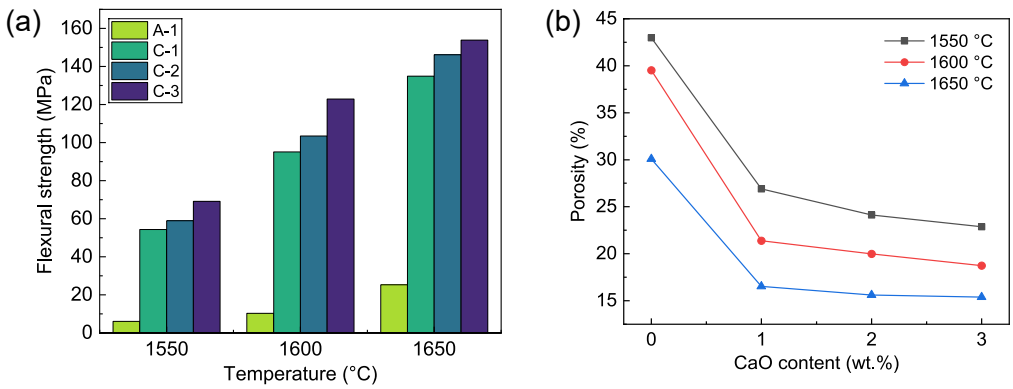

Fig. 8: Flexural strength (a) and porosity (b) of alumina ceramics with different CaO contents at 1,550 °C and 1,600 °C

strength. Simultaneously, the retained flaky grains and coarse particles preserve the porous structure and limit the shrinkage of alumina samples. Thus, doping with CaO sintering aids is crucial for producing alumina cores with qualified performance. However, given the significant enhancement effect, fine-tuning the doping content and optimizing the sintering temperature are essential for further improving the overall performance of the alumina ceramic cores.

4 Conclusions

Ceramic stereolithography technology was employed to manufacture CaO-doped alumina ceramic cores. Samples with varying doping amounts and sintering temperatures were characterized for their micro and macro performance, and their results were compared with those of cores made using other sintering aids. The following conclusions are drawn:

(1) In CaO-doped alumina ceramics prepared via stereolithography technology, CaO doping can induce changes in surface charge distribution and lattice structure of Al_2O_3, affecting surface energy states and interactions with other substances. The introduction of CaO can add atoms or ions to the alumina crystal structure, modifying its chemical properties. These chemical alterations may lead to variations in surface energy, disrupting the Wulff equilibrium, which in turn affects the sintering behavior of fine alumina particles, inhibiting the transformation of spherical fine particles into flaky grains. The retained spherical fine particles enhance sintering activity, thereby increasing flexural strength, while the retained flaky grains and coarse particles preserve the porous structure, limiting the shrinkage of alumina samples to some extent.

(2) By adjusting the CaO doping content and sintering temperature, sintering in an air atmosphere (>1,500 °C) effectively enhances the flexural strength of alumina cores. The impact of CaO doping is significant, as it enables the porosity of alumina cores to be maintained between 20% and 30%, and the sintering shrinkage rate is controlled to approximately 5% under sintering at 1,600 °C with 1% CaO doping.

(3) Considering the shrinkage rate, porosity, and mechanical properties of alumina ceramic cores, CaO doping significantly enhances their strength but negatively impacts shrinkage rate and porosity. Consequently, although the current limitations in shape and dimensional control of alumina cores hinder the efficient production of high-precision ceramic cores for industrial applications, the fabricated cores remain valuable for experimental research. For instance, they can be utilized to validate critical performance parameters such as leachability (core removal efficiency), thermal stability under high-temperature conditions, and mechanical strength. Additionally, these cores provide essential data for optimizing sintering parameters, compositional adjustments, and defect mitigation strategies, thereby guiding future improvements in precision and reliability.

Acknowledgments

This work was financially supported by the National Key R&D Program of China (No. 2023YFB4606101), the National Key R&D Program of China (No. 2022YFB4601404), the Innovative and Entrepreneurial PhD Program of Jiangsu Province (No. JSSCBS20210836), the youth program of Jiangnan University (No. JUSRP121038), the Taihu Talent Program of Wuxi City, and the Innovative and Entrepreneurial Talent Program of Jiangsu Province (No. JSSCRC2021531).

Conflict of interest

The authors declare that they have no known competing financial interests or personal relationships that could have appeared to influence the work reported in this paper.

References

[1] Kanyo J E, Schafföner S, Uwanyuze R S, et al. An overview of ceramic molds for investment casting of nickel superalloys. Journal of the European Ceramic Society, 2020, 40(15): 4955–4973.

[2] Lu G, Chen Y S, Yan Q S, et al. Investigation of microstructure and properties in short carbon fiber reinforced silica-based ceramic cores via atmosphere sintering. Journal of the European Ceramic Society, 2021, 41(14): 7339–7347.

[3] Wu H H, Li D C, Tang Y P, et al. Improving high temperature properties of alumina based ceramic cores containing yttria by vacuum impregnating. Materials Science and Technology, 2011, 27(4): 823–828.

[4] Li H, Liu Y, Colombo P, et al. The influence of sintering procedure and porosity on the properties of 3D printed alumina ceramic cores. Ceramics International, 2021, 47(19): 27668–27676.
[5] Li X, Su H, Dong D, et al. Enhanced comprehensive properties of stereolithography 3D printed alumina ceramic cores with high porosities by a powder gradation design. Journal of Materials Science & Technology, 2022, 131: 264–275.
[6] Wereszczak A, Breder K, Ferber M, et al. Dimensional changes and creep of silica core ceramics used in investment casting of superalloys. Journal of Materials Science, 2002, 37(19): 4235–4245.
[7] Li H, Liu Y S, Liu Y S, et al. Influence of debinding holding time on mechanical properties of 3D-printed alumina ceramic cores. Ceramics International, 2021, 47(4): 4884–4894.
[8] Li H, Liu Y S, Li W B, et al. The effect of sintering on the properties of CaO promoted alumina-based ceramic cores via 3D printing. Materials Chemistry and Physics, 2021, 263: 124443.
[9] Schileo G. Recent developments in ceramic multiferroic composites based on core/shell and other heterostructures obtained by sol-gel routes. Progress in Solid State Chemistry, 2013, 41(4): 87–98.
[10] Ozkan B, Sameni F, Goulas A, et al. Hot ceramic lithography of silica-based ceramic cores: the effect of process temperature on vat-photopolymierisation. Additive Manufacturing, 2022, 58: 103033.
[11] Xie R, Zhou K, Gan X, et al. Effects of epoxy resin on gelcasting process and mechanical properties of alumina ceramics. Journal of the American Ceramic Society, 2013, 96(4): 1107–1112.
[12] Hu F, Liu W, Xie Z. Surface modification of alumina powder particles through stearic acid for the fabrication of translucent alumina ceramics by injection molding. Ceramics International, 2016, 42(14): 16274–16280.
[13] Li J, An X, Liang J, et al. Recent advances in the stereolithographic three-dimensional printing of ceramic cores: Challenges and prospects. Journal of Materials Science & Technology, 2022, 117: 79–98.
[14] Chen Z, Li Z, Li J, et al. 3D printing of ceramics: A review. Journal of the European Ceramic Society, 2019, 39(4): 661–687.
[15] Li S, Duan W, Zhao T, et al. The fabrication of SiBCN ceramic components from preceramic polymers by digital light processing (DLP) 3D printing technology. Journal of the European Ceramic Society, 2018, 38(14): 4597–4603.
[16] Zhang F, Zhu L Y, Li Z G, et al. The recent development of vat photopolymerization: A review. Additive Manufacturing, 2021, 48: 102423.
[17] Tang W, Zhao T, Dou R, et al. Additive manufacturing of low-shrinkage alumina cores for single-crystal nickel-based superalloy turbine blade casting. Ceramics International, 2022, 48(11): 15218–15226.
[18] Wang R F, Zhang D M, Zhuang O Y, et al. Effect of Y_2O_3 content on the properties of alumina-based ceramic cores. Applied Mechanics and Materials, 2014, 488–489: 145–149.
[19] Tang S, Yang L, Liu X, et al. Direct ink writing additive manufacturing of porous alumina-based ceramic cores modified with nanosized MgO. Journal of the European Ceramic Society, 2020, 40(15): 5758–5766.
[20] Peng L, Jiang W, Yang L, et al. Effect of silica sol on performance and surface precision of alumina ceramic shell prepared by binder jetting. Ceramics International, 2022, 48(17): 24372–24382.
[21] Milak P, Minatto F D, Faller C, et al. The influence of dopants in the grain size of alumina–A review. Materials Science Forum, 2015, 820: 280–284.
[22] Kleinlogel C, Gauckler L J. Sintering and properties of nanosized ceria solid solutions. Solid State Ionics, 2000, 135(1–4): 567–573.
[23] Amsif M, Marrero-López D, Ruiz-Morales J, et al. Effect of sintering aids on the conductivity of $BaCe_{0.9}Ln_{0.1}O_{3-\delta}$. Journal of Power Sources, 2011, 196(22): 9154–9163.
[24] Liu J, Li Q, Huo M, et al. Microstructure and mechanical properties of 3D-printed nano-silica reinforced alumina cores. Ceramics International, 2022, 48(20): 30282–30293.
[25] Mächler D, Töpfer J. Effect of SiO_2 sintering additive on the positive temperature coefficient of resistivity (PTCR) behavior of $(Bi_{1/2}Na_{1/2})_{0.10}Ba_{0.90}TiO_3$+CaO ceramics. Materials Research Bulletin, 2017, 89: 217–223.
[26] Frueh T, Marker C, Kupp E R, et al. Powder chemistry effects on the sintering of MgO-doped specialty Al_2O_3. Journal of the American Ceramic Society, 2018, 101(7): 2739–2751.
[27] Johnson W, Coble R. A test of the second-phase and impurity-segregation models for MgO-enhanced densification of sintered alumina. Journal of the American Ceramic Society, 1978, 61(3–4): 110–114.
[28] Berry K A, Harmer M P. Effect of MgO solute on microstructure development in Al_2O_3. Journal of the American Ceramic Society, 1986, 69(2): 143–149.
[29] Bateman C A, Bennison S J, Harmer M P, et al. Mechanism for the role of magnesia in the sintering of alumina containing small amounts of a liquid phase. Journal of the American Ceramic Society, 1989, 72(7): 1241–1244.
[30] Arab A, Sktani Z D I, Zhou Q, et al. Effect of MgO addition on the mechanical and dynamic properties of zirconia toughened alumina (ZTA) ceramics. Materials, 2019, 12(15): 2440.
[31] Handwerker C A, Morris P A, Coble R L. Effects of chemical inhomogeneities on grain growth and microstructure in Al_2O_3. Journal of the American Ceramic Society, 1989, 72(1): 130–136.
[32] Shabani S, Naghizadeh R, Vostakola M F, et al. The effect of MgO addition on the properties of alumina-based ceramic cores prepared via sol-gel process. Journal of Sol-Gel Science and Technology, 2020, 96(3): 539–549.
[33] Williams J C, Boyer R R. Opportunities and issues in the application of titanium alloys for aerospace components. Metals, 2020, 10(6): 705.
[34] Li H, Liu Y S, Li W B, et al. The effect of sintering on the properties of calcium oxide promoted alumina-based ceramic cores via 3D printing. Materials Chemistry and Physics, 2021, 263: 124443.
[35] Qian C, Hu K, Shen Z, et al. Effect of sintering aids on mechanical properties and microstructure of alumina ceramic via stereolithography. Ceramics International, 2023, 49(11): 17506–17523.
[36] Yuan C, Wang F, Qi B, et al. 3D printing of multi-material composites with tunable shape memory behavior. Materials & Design, 2020, 193: 108785.
[37] Baca D, Ahmad R. The impact on the mechanical properties of multi-material polymers fabricated with a single. The International Journal of Advanced Manufacturing Technology, 2020, 106(9): 4509–4520.
[38] Li X, Su H, Dong D, et al. Enhanced comprehensive properties of stereolithography 3D printed alumina ceramic cores. Journal of Materials Science & Technology, 2022, 131: 264–275.
[39] Pan Y, Li H, Liu Y S, et al. Effect of holding time during sintering on microstructure and properties of 3D printed alumina ceramics. Frontiers in Materials, 2020, 7: 54.
[40] Peng L, Jiang W M, Yang L, et al. Effect of silica sol on performance and surface precision of alumina ceramic. Ceramics International, 2022, 48(17): 24372–24382.
[41] Qiu Y, Li Q, Yang K, et al. Thermal shock resistant 3D printed ceramics reinforced with $MgAl_2O_4$ shell structure. Journal of Materials Science & Technology, 2024, 178: 100–111.
[42] Zhai X, Chen J, Su R, et al. Vat photopolymerization 3D printing of Al_2O_3 ceramic cores with strip-shaped pores by using polyamide 6 fiber template. Journal of the American Ceramic Society, 2024, 107(8): 5400–5411.
[43] Zhang K, Meng Q, Qu Z, et al. A review of defects in vat photopolymerization additive-manufactured ceramics: Characterization, control, and challenges. Journal of the European Ceramic Society, 2024, 44(3): 1361–1384.
[44] Zhang K, Meng Q, Zhang X, et al. Quantitative characterization of defects in stereolithographic additive manufactured ceramic using X-ray computed tomography. Journal of Materials Science & Technology, 2022, 118: 144–157.